

Polarization conversion effect in cholesteric liquid crystal-based polarization volume gratings

YUQIANG DING, YEFU ZHANG, YONGZIYAN MA, YUGE HUANG, AND SHIN-TSON WU* 

College of Optics and Photonics, University of Central Florida, Orlando, FL 32816, USA

**swu@creol.ucf.edu*

Abstract: Following the recent experimental discovery of a new polarization conversion phenomenon in polarization volume gratings (PVGs), in this paper, we investigate its underlying physical mechanisms in cholesteric liquid crystal (CLC) reflectors and PVGs. We examine the transition of eigenstates from circular to linear polarization as the incident angle deviates from the helical axis, which originates such an anomalous polarization conversion effect. While this transition enables PVGs to double the in-coupling efficiency and brightness uniformity in waveguide-based augmented reality (AR) displays, it also degrades the polarization selectivity and alters the transmitted polarization state in both CLC reflectors and PVGs, which in turn narrows down their spectral and angular bandwidth in the multi-layer design. These findings help not only deepen the understanding of polarization behaviors in CLC-based optical elements but also provide valuable insights to optimize their performances for emerging AR smart glasses.

© 2024 Optica Publishing Group under the terms of the [Optica Open Access Publishing Agreement](#)

1. Introduction

Cholesteric liquid crystals (CLCs) naturally form a self-organized helical structure, which can be viewed as a one-dimensional photonic crystal [1–6]. The sinusoidal rotation of the CLC directors creates a periodic variation in permittivity, leading to a polarization-sensitive photonic bandgap. Within this photonic bandgap, circularly polarized light with the same handedness as the CLC helix is selectively reflected, particularly for the wavelengths near the helical pitch length. Such a reflection band, commonly known as selective reflection, depends on the pitch length and birefringence of the CLC. The selective reflection bandwidth can be precisely controlled by adjusting the chiral dopant concentration in the CLC mixture. The unique optical properties have made CLCs essential in various practical applications, including reflective displays, circular polarizers, mirrors, and lasers [7–15]. Recent advances in patterned alignment technology have significantly enhanced the capabilities of CLCs, particularly in controlling the phase of reflected light. This innovation has led to the development of new diffractive optical components [16,17]. Among these advancements, patterned CLCs are emerging as essential elements for next-generation virtual reality (VR) and augmented reality (AR) displays. A noteworthy innovation in this area is the polarization volume grating (PVG) [18–29], which features a linear CLC director variation along the azimuthal direction. This unique patterning results in slanted periodic CLC layers, enabling highly efficient light diffraction into a single diffraction order. Waveguide-based AR displays using PVGs are currently under active development [22–27,29,30], highlighting their potential for high efficiency, strong polarization selectivity, dynamic switching capabilities, straightforward fabrication processes, and cost-effectiveness, while improving the optical performance for AR and VR displays.

In a recent study, an anomalous polarization conversion phenomenon was experimentally observed in the PVG during multiple interactions in waveguide-based AR displays [26]. This novel polarization conversion phenomenon has enabled PVGs to break the theoretical in-coupling

efficiency limits of traditional waveguide-based AR displays, establishing PVGs as a promising high-efficiency coupler. However, the underlying mechanisms of this phenomenon have yet to be fully understood.

In this paper, we thoroughly investigate the polarization conversion phenomenon in CLC reflectors and PVGs, focusing on their polarization properties both analytically and numerically. Our analysis reveals that such a polarization conversion is inherently tied to all CLC-based devices, including CLC reflectors and CLC-based polarization volume holograms. We find that this phenomenon is triggered by the transition of eigenstates from circular polarization to linear polarization as the incident angle deviates from the helical axis. While this polarization conversion enhances the PVG performance in waveguide displays, it also introduces some challenges, such as polarization degradation, that can deteriorate the angular and spectral responses of multi-layer structures. Overall, our findings not only offer new insights into the polarization properties of CLC-based devices but also provide practical guidelines to optimize these devices for various applications, including imaging systems and AR/VR displays.

2. Polarization properties in CLC reflectors

2.1. Optical properties in CLC reflectors at normal incidence

Before discussing oblique incidence, we first examine the optical properties of CLC reflectors at normal incidence, where analytical solutions are available. By analyzing light propagation along the optical axis of a CLC reflector in this simpler case, we gain valuable insights that form the foundation for understanding the more complex behavior of CLC reflectors and PVGs under oblique incidence, as explored in the following sections.

The optical properties of CLCs are most naturally described by solving Maxwell's equations, with the dielectric properties of the CLC represented by a coordinate-dependent dielectric tensor, $\hat{\epsilon}(z)$:

$$\hat{\epsilon}(z) = \begin{pmatrix} \bar{\epsilon} + \bar{\epsilon}\delta \cos(\tau z) & \pm \bar{\epsilon}\delta \sin(\tau z) & 0 \\ \pm \bar{\epsilon}\delta \sin(\tau z) & \bar{\epsilon} - \bar{\epsilon}\delta \cos(\tau z) & 0 \\ 0 & 0 & 1 \end{pmatrix}, \quad (1)$$

where the z -axis lies along the optical axis, $\tau = 4\pi/p$ (with p as the CLC pitch length), $\epsilon_1 = n_e^2$ and $\epsilon_2 = \epsilon_3 = n_o^2$ are the principal values of the dielectric-constant tensor, $\bar{\epsilon} = (\epsilon_1 + \epsilon_2)/2$, and $\delta = (\epsilon_1 - \epsilon_2)/(\epsilon_1 + \epsilon_2)$. The signs in this expression correspond to the two possible geometric configurations: positive sign for a right-handed cholesteric helix and negative sign for a left-handed cholesteric helix. The coordinate dependence of the tensor $\hat{\epsilon}(z)$ reflects the point-to-point variation in the orientation of the principal axes, determined by the local alignment of the CLC directors.

Building on previous work [1,4,6], we derive the solution to Maxwell's equations for a CLC reflector with the dielectric permittivity defined earlier, assuming a right-handed cholesteric helix (positive sign). For a wave propagating along the helical axis, the wave equation is given by:

$$\frac{\partial^2 \vec{E}}{\partial z^2} = \frac{\hat{\epsilon}}{c^2} * \frac{\partial^2 \vec{E}}{\partial t^2}, \quad (2)$$

where the z -axis lies along the optical axis, and \vec{E} represents the electric field vector, which is perpendicular to the z -axis. The eigenwave in the CLC can be expressed as a superposition of two circularly polarized plane waves:

$$\vec{E} = \vec{n}_+ E_+ \exp \left[i \left(\beta + \frac{\tau}{2} \right) z - i\omega t \right] + \vec{n}_- E_- \exp \left[i \left(\beta - \frac{\tau}{2} \right) z + i\omega t \right], \quad (3)$$

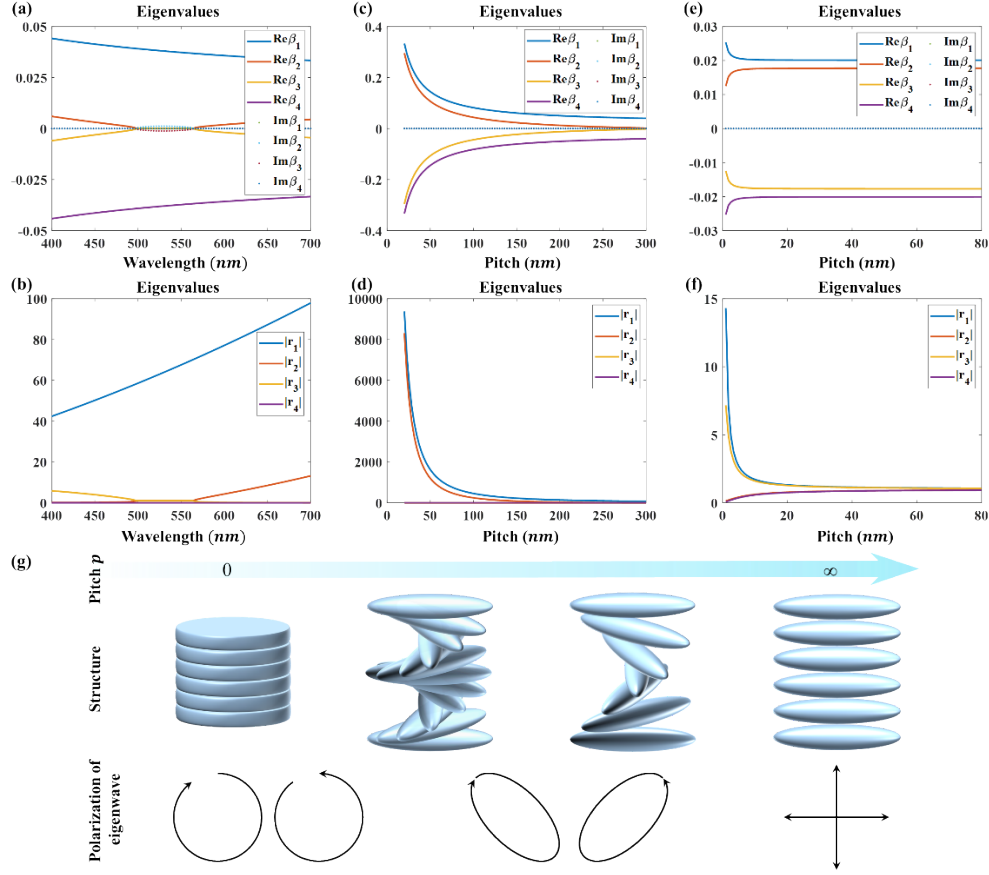


Fig. 1. Eigenwaves and Eigenvalues in CLC reflectors at normal incidence. (a) Variation of eigenvalues with wavelength around the photonic bandgap. (b) Ratio of LCP to RCP light in each eigenwave as a function of wavelength around the photonic bandgap. (c) Variation of eigenvalues with short CLC pitches. (d) Ratio of LCP to RCP light in each eigenwave for short CLC pitches. (e) Variation of eigenvalues with long CLC pitches. (f) Ratio of LCP to RCP light in each eigenwave for long CLC pitches. (g) Evolution of liquid crystal structures and the polarization of their corresponding eigenwaves with varying pitch at normal incidence. The CLC pitch used in (a-b) is 332.5 nm, while the simulated wavelength in (c-f) is 532 nm. The refractive indices of the liquid crystal are $n_e = 1.7$ and $n_o = 1.5$.

where $\vec{n}_{\pm} = (\vec{e}_x \pm i\vec{e}_y)/\sqrt{2}$ are the circular-polarization unit vectors, ω is the frequency of light, and β is the propagation constant of the eigenwaves. Substituting Eq. (3) into the wave equation (Eq. (2)), we arrive at the following system of equations for the amplitudes E_+ and E_- :

$$\left[k^2 - \left(\beta + \frac{\tau}{2} \right)^2 \right] E_+ + k^2 \delta E_- = 0, \quad (4)$$

$$k^2 \delta E_+ + \left[k^2 - \left(\beta - \frac{\tau}{2} \right)^2 \right] E_- = 0, \quad (5)$$

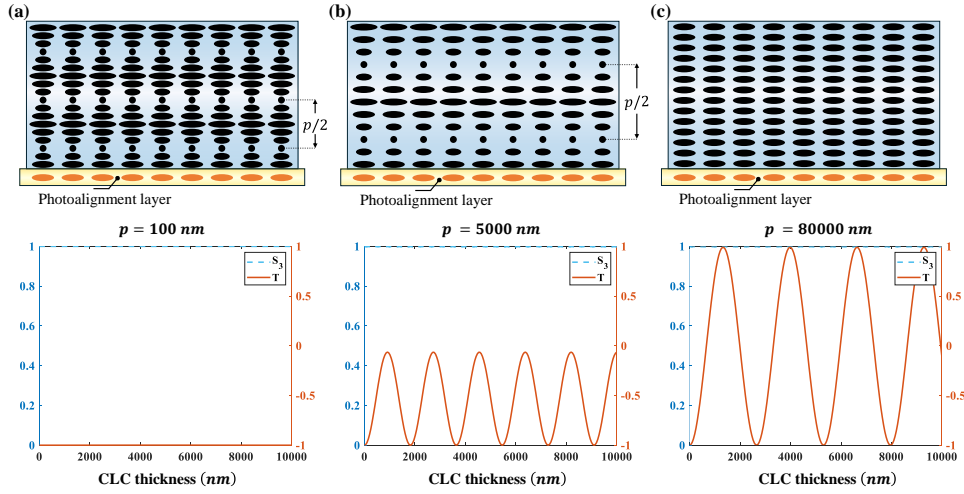


Fig. 2. Transition of eigenwaves in CLC reflectors with varying pitches at normal incidence. (a) Polarization conversion as a function of thickness in CLC reflectors with a 100-nm pitch. (b) Polarization conversion as a function of thickness in CLC reflectors with a 5- μm pitch. (c) Polarization conversion as a function of thickness in CLC reflectors with an 80- μm pitch.

where $k^2 = \bar{\epsilon}\omega^2/c^2$. From Eq. (4) and Eq. (5), by eliminating E_-/E_+ we obtain the following eigenvalue equation:

$$\left[k^2 - \left(\beta + \frac{\tau}{2} \right)^2 \right] \left[k^2 - \left(\beta - \frac{\tau}{2} \right)^2 \right] - k^4 \delta^2 = 0. \quad (6)$$

Solving Eq. (6) yields the following eigenvalues:

$$\beta_j = \pm \sqrt{k^2 + \frac{\tau^2}{4} \pm k\sqrt{\tau^2 + k^2\delta^2}}, \quad j = 1, 2, 3, 4; \quad (7)$$

where ++, +-, --, -+ represent 1st, 2nd, 3rd, and 4th eigenvalues, respectively. For a given frequency ω (or wavelength λ), these four solutions correspond to four possible eigenwaves, each with a unique ratio of amplitudes E_+ and E_- , given by:

$$r_j = \left(\frac{E_-}{E_+} \right)_j = \frac{k^2 \delta}{(\beta_j - \frac{\tau}{2})^2 - k^2}. \quad (8)$$

According to Eq. (7), the eigenvalues for solutions 2 and 3 become imaginary near the Bragg frequency $\omega_B = \frac{\tau c}{2\sqrt{\bar{\epsilon}}}$ (or Bragg wavelength $\lambda_B = p\sqrt{\bar{\epsilon}}$), within the frequency range $\frac{\omega_B}{\sqrt{1+\delta}} < \omega < \frac{\omega_B}{\sqrt{1-\delta}}$ (or $pn_o < \lambda_B < pn_e$). In this range, the corresponding circularly polarized waves cannot propagate in the crystal, resulting in a photonic bandgap, as Fig. 1(a) depicts. Since eigenwaves 1 and 4 are closely aligned with the left-handed circular polarization state as shown in Fig. 1(b), while eigenwaves 2 and 3 are prohibited from propagating due to their imaginary eigenvalues, most right-handed circular polarization is reflected, whereas most left-handed circular polarization transmits through the CLC. This behavior explains the circular polarization selectivity observed in CLC reflectors.

Here, we primarily focus on the region outside the bandgap, where nearly all light passes through the CLC. To investigate the polarization conversion in this region, we first consider two extreme cases: when the optical pitch of the CLC approaches infinity or zero.

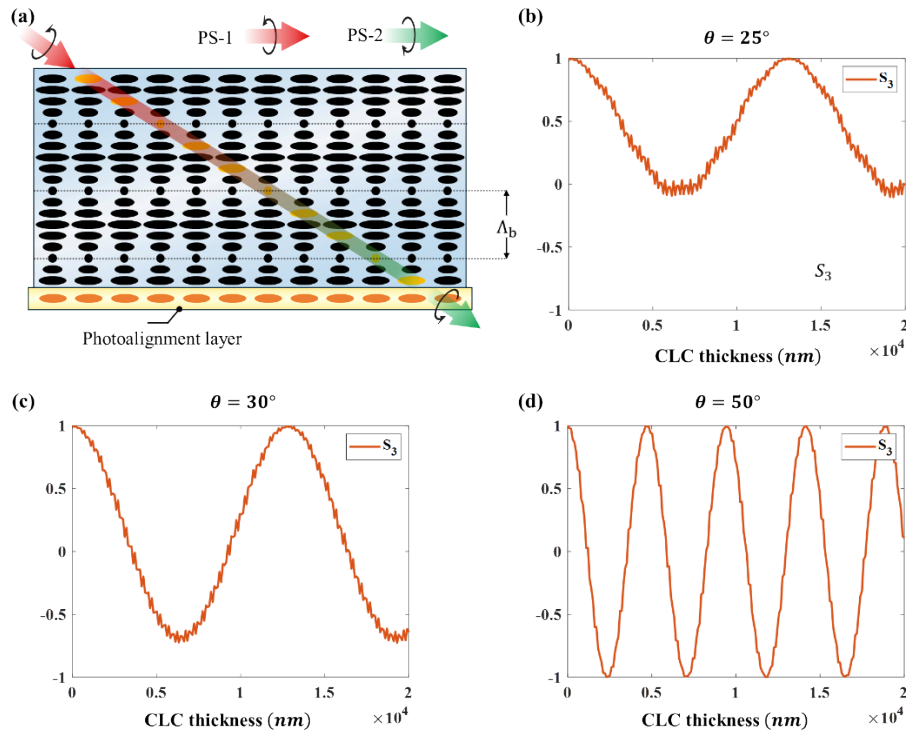


Fig. 3. Polarization conversion in CLC at large incident angles. (a) Schematic illustration of polarization conversion in CLC. Polarization conversion as a function of PVG thickness at incident angles (b) $\theta = 25^\circ$, (c) $\theta = 30^\circ$, (d) $\theta = 50^\circ$ in a glass substrate, for $\lambda = 532$ nm. The CLC pitch is 332.5 nm, with LC refractive indices $n_e = 1.7$ and $n_o = 1.5$. PS indicates polarization state in (a).

In the first extreme case, when the optical pitch of the CLC reflector approaches zero ($p \ll \lambda$), the forward eigenwaves approach to left-handed circular polarization state and right-handed circular polarization state with same eigenvalues as shown in Fig. 1(c-d). As a result, any incident polarization state is preserved as it passes through the CLC. For instance, if an LCP light is incident on the crystal, the normalized Stokes parameter $S_3 = -2\text{Im}(E_x E_y^*) / (|E_x|^2 + |E_y|^2)$ remains constant with increasing thickness. To validate this explanation, we employ the 4×4 matrix method [31] for CLC reflectors with a pitch of 100 nm, as shown in Fig. 2(a), which aligns well with our findings. Furthermore, in this extremely short pitch case, the CLC can be effectively treated as a negative C-plate [32], characterized by an effective extraordinary refractive index given by:

$$n_{ee} = \frac{1}{2\pi} \int_0^{2\pi} \sqrt{n_e^2 \cos^2 \phi + n_o^2 \sin^2 \phi} d\phi. \quad (9)$$

In the second case, as the optical pitch of the CLC reflectors approaches infinity ($p \gg \lambda$), the CLC effectively behaves like a homogeneous waveplate. In this scenario, the forward eigenwaves correspond to s-polarization and p-polarization states with distinct eigenvalues as shown in Fig. 1(e-f). Consequently, the phase difference between these eigenwaves accumulates with increasing thickness of the CLC. When an LCP light is incident on the crystal, the Stokes parameter S_3 oscillates between -1 and 1 as the thickness increases. To validate this explanation, we implement simulation for a CLC reflectors with a pitch of 80 μm , as shown in Fig. 2(c), which aligns well with our findings.

Between these two extreme conditions, the amplitude ratios r_j of the forward eigenwaves gradually decrease and converge toward 1 as the pitch increases, as shown in Fig. 1(f). This suggests a transition of the polarization states of the forward eigenwaves from circular to linear polarization. For example, when an LCP light is incident on a CLC with a medium optical pitch of $5 \mu\text{m}$, the Stokes parameter S_3 oscillates from -1 to a value less than 1 as the thickness increases, as illustrated in Fig. 2(b). Overall, as illustrated in Fig. 1(g), the polarization of eigenwaves gradually evolve from circular to linear polarization states as the optical pitch increases.

2.2. Polarization conversion in CLC reflectors at oblique incidence

Similarly, in a CLC reflector designed for a specific wavelength (e.g., $\lambda_B = 532 \text{ nm}$) at normal incidence, we observe a similar phenomenon when the oblique incident angle θ falls outside the photonic bandgap (or Bragg region). As the incident angle increases, the eigenstates gradually transition from circular to linear polarization. Since the eigenfunctions cannot be analytically solved at oblique incidence, we numerically simulate the optical response for various incident angles. For relatively small angles (e.g., $\theta = 25^\circ$ in surrounding medium with a refractive index of 1.6), the incident light perceives a longer pitch, as illustrated in Fig. 3(a). The simulation results in Fig. 3(b) show that the Stokes parameter S_3 oscillates from 1 to a value larger than -1 as the CLC thickness increases, indicating that the eigenwaves are in an elliptical polarization

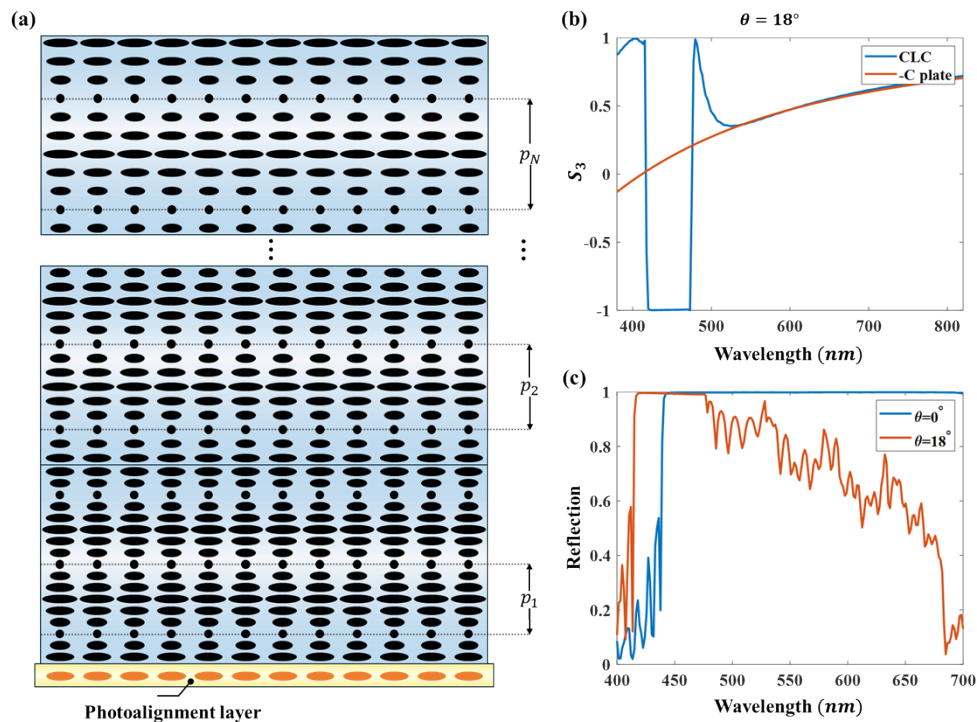


Fig. 4. Polarization degradation in CLC reflectors at oblique incidence. (a) Multi-layer structure of CLC reflectors. (b) Stokes parameter S_3 of the transmitted light at an incidence angle of $\theta = 18^\circ$ in a glass substrate. (c) Spectral response of reflection in multi-layer CLC reflectors at incidence angles of $\theta = 0^\circ$ and $\theta = 18^\circ$. The CLC pitch and thickness used in (b) are 293.75 nm and $9 \mu\text{m}$, respectively. The CLC pitches used in (c) are 293.75 nm , 325 nm , 356.25 nm , 387.5 nm , and 418.75 nm , with each layer having a thickness of $5 \mu\text{m}$. The refractive indices of the liquid crystal are $n_e = 1.7$ and $n_o = 1.5$.

state. As shown in Fig. 3(c-d), with increasing incident angles, the Stokes parameters transition more completely from 1 to -1 , signifying that the eigenstates evolve towards linear polarization, specifically the s and p waves.

While the polarization conversion in an CLC reflector is intriguing, it notably compromises the spectral performance of a broadband CLC reflector at oblique incidence. In a multi-layer broadband CLC reflector [9,33,34], as shown in Fig. 4(a), each layer modifies the transmitted light's polarization state due to this conversion (Fig. 4(b)), similar to the effect of a negative C-plate discussed earlier. This progressive alteration in polarization reduces the reflection efficiency in subsequent layers. Consequently, as the central wavelength of the CLC layers increases from the bottom to the top in Fig. 4(a), the reflection efficiency gradually declines, as shown in Fig. 4(c). This degradation in angular performance also occurs in gradient-pitch broadband CLC reflectors, albeit with a more gradual efficiency drop. To enhance the angular performance in broadband CLC reflectors, future developments should focus on polarization compensation films or innovative CLC structures [35].

3. Polarization properties in PVGs

3.1. Polarization degradation in PVGs around normal incidence

PVG is a polarization-selective holographic optical element that records the polarization information of two interfering beams: RCP and LCP. As shown in Fig. 5(a), the PVG features a slanted CLC structure, where the liquid crystal directors rotate along the helical axis. This CLC structure imparts polarization-selective characteristics to the PVG, enabling it to reflect circular polarization states that match the handedness of the helical twist while transmitting the opposite component. For instance, it diffracts the LCP light while allowing the RCP light to pass through.

However, the slanted CLC structure also leads to degraded circular polarization selectivity in the PVG in comparison with an CLC reflector at normal incidence. Interestingly, this polarization selectivity is not uniform across different incident angles, even within the photonic bandgap. As the incident angle deviates from the helical axis, the circular polarization response of the PVG gradually deteriorates. Because the eigenfunction of the PVG is not analytically solvable, we utilize RCWA model [36] to simulate its optical response. For instance, let us consider a PVG with a horizontal period of 400 nm and a slant angle of 28.96° (corresponding to a central wavelength of 532 nm). As illustrated in Fig. 5(b), as the incident angle departs from the helical axis toward the Bragg plane, the diffraction efficiency of the RCP light decreases, even at a very large thickness, while the LCP light starts to show a diffraction response. This trend signifies a declined polarization selectivity, primarily due to the slanted CLC structure. Our studies of CLC reflectors reveal that the eigenstates shift away from circular polarization as the incident angle increases. Therefore, the PVG achieves an optimal circular polarization response when the incident angle remains close to the helical axis, owing to the slanted structure.

Additionally, in contrast to an CLC reflector, PVGs exhibit polarization degradation in transmitted light even at normal incidence, primarily due to the slanted CLC structure, as Fig. 5(c) shows. This degradation adversely affects not only the angular response but also the spectral performance of multi-layer PVGs. For instance, when using multi-layer or gradient-pitch PVGs [22,25,27,37,38] to achieve broadband performance, this polarization degradation can significantly reduce the diffraction efficiency of the upper layers, even at normal incidence as depicted in Fig. 5(d). Fortunately, most applications do not require extremely high diffraction efficiency (e.g., 99.9%), so a thinner PVG with lower efficiency can still be used without a significant polarization degradation. Therefore, multi-layer PVGs with moderate efficiency remain feasible.

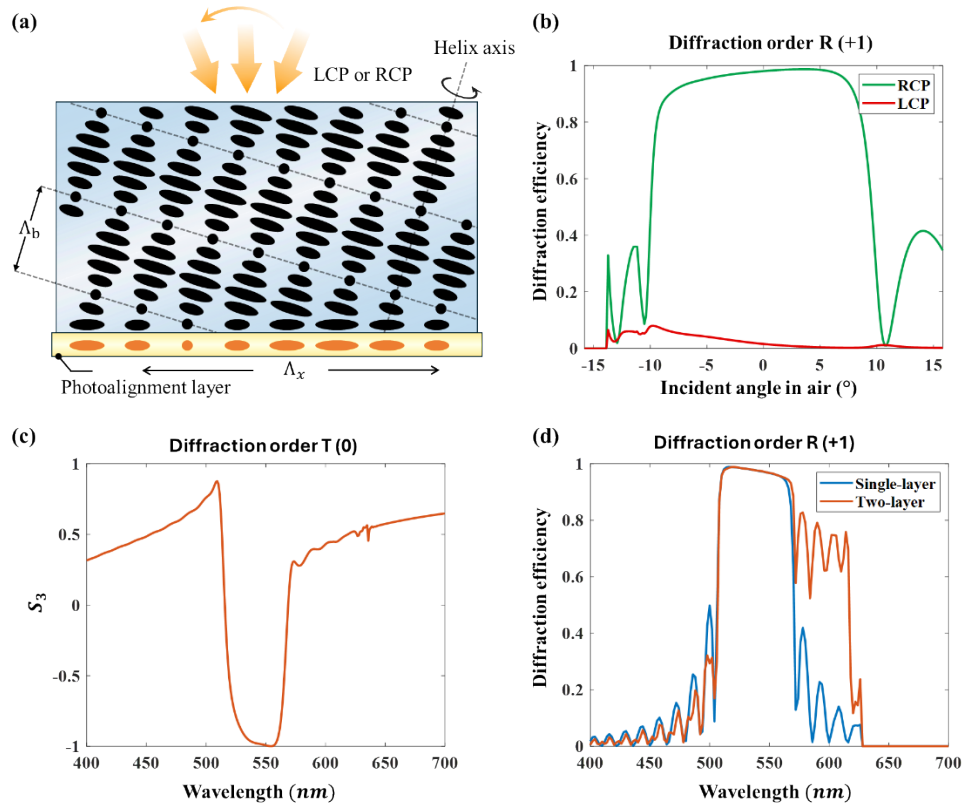


Fig. 5. Polarization degradation in PVG around normal incidence. (a) The slanted structure of PVG. (b) Angular response of diffraction order R (+1) in PVG at normal incidence with a wavelength of 532 nm for both LCP and RCP light. (c) Stokes parameter S_3 of the transmitted light (diffraction order T (0)) at normal incidence. (d) Spectral response of diffraction order R (+1) in single-layer and two-layer PVGs at normal incidence. The single-layer PVG in (b-d) has a horizontal period of 400 nm, a thickness of 3.5 μm , and a slant angle of 28.96°. The two-layer PVG in (d) features the same horizontal period, with thicknesses of 3.5 μm and slant angles of 28.96° and 33.75° for each layer. The refractive indices of the liquid crystal are $n_e = 1.7$ and $n_o = 1.5$.

3.2. Optical conversion in PVGs at oblique incidence

As the incident angle increases toward the Bragg plane, the incident light may no longer satisfy the Bragg conditions, which in turn experiences a phase mismatching described by following equation:

$$\left| n_{in} \sin \theta_{in} - \frac{\lambda}{\Lambda_x} \right| > |n_{out}|, \quad (10)$$

where n_{in} and n_{out} are the refractive indices of the input and output media, θ_{in} is the incident angle, λ is the wavelength, and Λ_x is the horizontal period of the PVG. In this scenario, nearly all light will pass through the PVG, and polarization conversion begins to occur. For example, when the incident angle is relatively small (e.g., $\theta = -11^\circ$ in the glass with a refractive index of 1.57), the incident light perceives a longer pitch, as illustrated in Fig. 6(a). The simulation results in Fig. 6(b) indicate that the Stokes parameter S_3 oscillates from -1 to a value less than 1 as the PVG thickness increases, suggesting that the eigenwaves exhibit an elliptical polarization state. As Fig. 6(c-f) shows, increasing the incident angle allows the Stokes parameters to transition

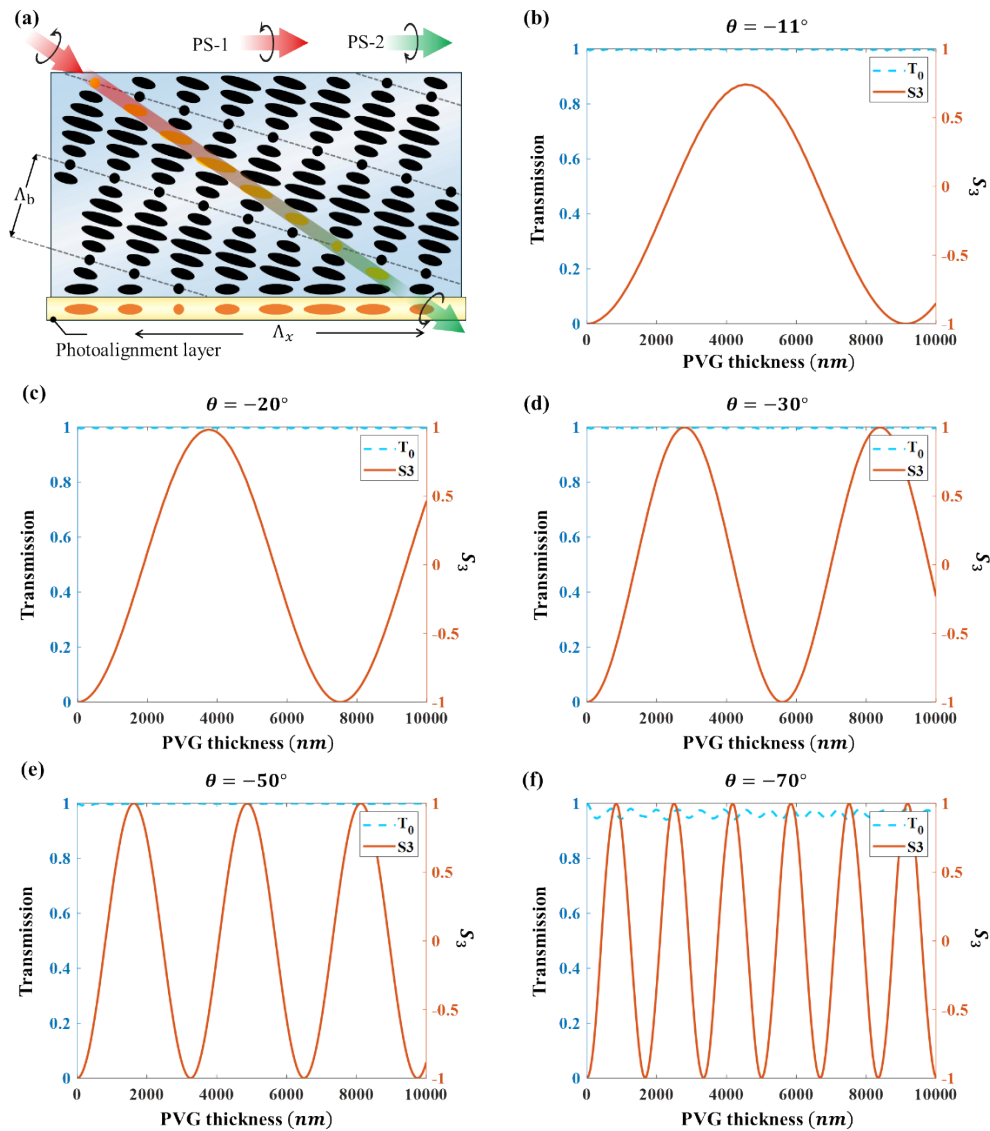


Fig. 6. Polarization conversion of PVG at large incident angles. (a) Schematic illustration of polarization conversion in a PVG. Simulated PVG thickness dependent polarization conversion at incident angle (b) $\theta = -11^\circ$, (c) $\theta = -20^\circ$, (d) $\theta = -30^\circ$, (e) $\theta = -50^\circ$, and (f) $\theta = -70^\circ$ in the glass substrate, for a wavelength of 532 nm. The horizontal period and slanted angle of the PVG is 400 nm and 28.96° , respectively, and the LC refractive indices are $n_e = 1.7$ and $n_o = 1.5$. PS indicates polarization state in (a).

gradually from -1 to 1 , indicating a shift of eigenstates toward a linearly polarized light (s and p waves). Notably, the simulation reveals that PVG can achieve a complete circular polarization conversion at a smaller incident angle compared to an CLC reflector. This is primarily due to the slanted structure of the PVG, which provides a wider angular range for achieving a complete polarization conversion, thereby significantly enhancing the in-coupling efficiency in waveguide-based AR displays.

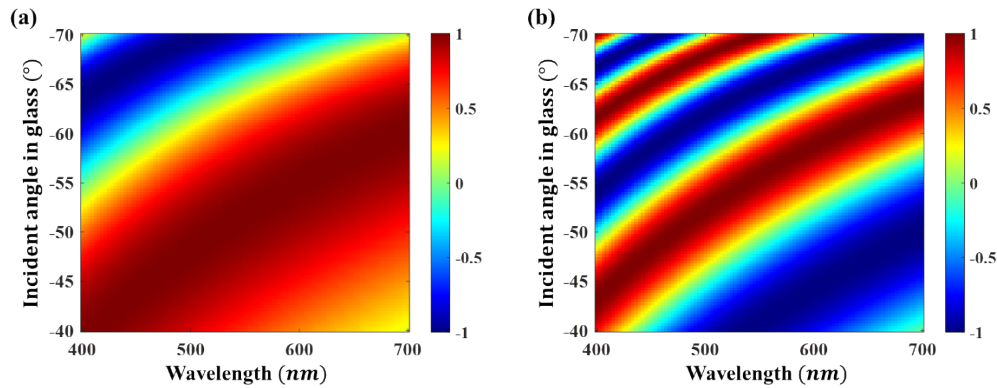


Fig. 7. Angular and spectral response of polarization conversion at (a) first-order half-wave phase retardation at PVG thickness of $1.6 \mu\text{m}$ and (b) second-order phase retardation at PVG thickness of $4.3 \mu\text{m}$. The horizontal period and slanted angle of the PVG is 400 nm and 28.96° , respectively, and the LC refractive indices are $n_e = 1.7$ and $n_o = 1.5$.

Furthermore, we also investigate the angular and spectral responses of PVGs. The results above indicate that PVGs can achieve a complete circular polarization conversion at multiple optimal thicknesses, akin to multiple-order half-wave phase retardations. However, as the order of phase retardation increases, corresponding to a greater optical thickness, the angular and spectral bandwidths of the circular polarization conversion become narrower. As shown in Fig. 7(a-b), a PVG at the first optimal thickness (first-order half-wave phase retardation) exhibits a significantly broader angular and spectral bandwidth compared to a PVG at the second optimal thickness (second-order half-wave phase retardation). However, neither can convert the polarization in the entire TIR angles for the visible light. Therefore, adding a polarization compensation film or modifying the device structure is required to achieve a broadband and wide-view polarization conversion. Additionally, like a conventional half-wave plate, increasing the LC birefringence does not expand the angular or spectral bandwidth. However, it does reduce the optical thickness required for each order of half-wave phase retardation, thereby lowering the fabrication complexity of PVGs. This is crucial since a thicker PVG film is more difficult to align well due to the limited anchoring energy provided by the photoalignment layer. In contrast, the diffraction of a transmissive PVG mainly relies on the half-wave condition, which can be naturally explained by the above-mentioned polarization conversion as well because it usually has a Bragg angle (or slanted angle) larger than 45 degrees, like the large incidence angle in a reflective PVG.

4. Conclusion

In summary, we have investigated the underlying mechanism of the recently observed anomalous polarization conversion in CLC reflectors and CLC-based PVGs. Our findings demonstrate that as the incident angle deviates from the helical axis, the eigenstates gradually shift from circular to linear polarization, resulting in an anomalous polarization conversion in both structures. While this transition enables PVGs to break the in-coupling efficiency limit in waveguide-based AR displays, it also reduces the polarization selectivity and alters the transmitted light's polarization state in CLC reflectors and PVGs, thereby impairing their spectral and angular performance in multi-layer broadband configurations. Overall, these physical insights contribute to a deeper understanding on the polarization behavior of CLC-based optical elements, which in turn offers valuable guidance to optimizing the CLC design for advanced optical applications.

Funding. Meta.

Acknowledgments. The UCF group is indebted to Meta Platforms for financial support and John Semmen for useful discussion.

Disclosures. The authors declare no conflicts of interest.

Data Availability. Data underlying the results presented in this paper are not publicly available at this time but may be obtained from the authors upon reasonable request.

References

1. D. K. Yang and S. T. Wu, "*Fundamentals of Liquid Crystal Devices*," 2nd Ed. (Wiley, 2014).
2. D. W. Berreman and T. J. Scheffer, "Bragg Reflection of Light from Single-Domain Cholesteric Liquid-Crystal Films," *Phys. Rev. Lett.* **25**(9), 577–581 (1970).
3. R. Dreher, G. Meier, and A. Saupe, "Selective Reflection by Cholesteric Liquid Crystals," *Mol. Cryst. Liq. Cryst.* **13**(1), 17–26 (1971).
4. E. I. Kats, "Optical properties of cholesteric liquid crystals," *Sov. Phys. Usp.* **32**(5), 1004–1007 (1971).
5. R. Dreher and G. Meier, "Optical Properties of Cholesteric Liquid Crystals," *Phys. Rev. A* **8**(3), 1616–1623 (1973).
6. V. A. Belyakov, V. E. Dmitrienko, and V. P. Orlov, "Optics of cholesteric liquid crystals," *Sov. Phys. Usp.* **22**(2), 64–88 (1979).
7. D. K. Yang, L. C. Chien, and J. W. Doane, "Cholesteric liquid crystal/polymer dispersion for haze-free light shutters," *Appl. Phys. Lett.* **60**(25), 3102–3104 (1992).
8. X. Zhu, Z. Ge, T. X. Wu, *et al.*, "Transflective Liquid Crystal Displays," *J. Disp. Technol.* **1**(1), 15–29 (2005).
9. D. J. Broer, J. Lub, and G. N. Mol, "Wide-band reflective polarizers from cholesteric polymer networks with a pitch gradient," *Nature* **378**(6556), 467–469 (1995).
10. R. A. M. Hikmet and H. Kemperman, "Electrically switchable mirrors and optical components made from liquid-crystal gels," *Nature* **392**(6675), 476–479 (1998).
11. V. I. Kopp, B. Fan, H. K. M. Vithana, *et al.*, "Low-threshold lasing at the edge of a photonic stop band in cholesteric liquid crystals," *Opt. Lett.* **23**(21), 1707–1709 (1998).
12. H. Finkelmann, S. T. Kim, A. Muñoz, *et al.*, "Tunable Mirrorless Lasing in Cholesteric Liquid Crystalline Elastomers," *Adv. Mater.* **13**(14), 1069–1072 (2001).
13. T. Matsui, R. Ozaki, K. Funamoto, *et al.*, "Flexible mirrorless laser based on a free-standing film of photopolymerized cholesteric liquid crystal," *Appl. Phys. Lett.* **81**(20), 3741–3743 (2002).
14. Y. Matsuhisa, Y. Huang, Y. Zhou, *et al.*, "Low-threshold and high efficiency lasing upon band-edge excitation in a cholesteric liquid crystal," *Appl. Phys. Lett.* **90**(9), 091114 (2007).
15. S. S. Choi, S. M. Morris, W. T. S. Huck, *et al.*, "Liquid Crystals: Electrically Tuneable Liquid Crystal Photonic Bandgaps," *Adv. Mater.* **21**(38-39), 3915–3918 (2009).
16. J. Xiong, K. Yin, K. Li, *et al.*, "Holographic Optical Elements for Augmented Reality: Principles, Present Status, and Future Perspectives," *Adv. Photonics Res.* **2**(1), 2000049 (2021).
17. Q. Yang, Y. Li, Y. Ding, *et al.*, "Compact Foveated AR Displays with Polarization Selective Planar Lenses," *ACS Appl. Opt. Mater.* **2**(7), 1347–1352 (2024).
18. J. Kobashi, H. Yoshida, and M. Ozaki, "Planar optics with patterned chiral liquid crystals," *Nat. Photonics* **10**(6), 389–392 (2016).
19. Y. Weng, D. Xu, Y. Zhang, *et al.*, "Polarization volume grating with high efficiency and large diffraction angle," *Opt. Express* **24**(16), 17746–17759 (2016).
20. I. Nys, M. Stebryte, Y. Ye, *et al.*, "Tilted Chiral Liquid Crystal Gratings for Efficient Large-Angle Diffraction," *Adv. Opt. Mater.* **7**(22), 1901364 (2019).
21. Y. H. Lee, Z. He, and S. T. Wu, "Optical properties of reflective liquid crystal polarization volume gratings," *J. Opt. Soc. Am. B* **36**(5), D9–D12 (2019).
22. X. Yan, J. Wang, W. Zhang, *et al.*, "Gradient polarization volume grating with wide angular bandwidth for augmented reality," *Opt. Express* **31**(21), 35282–35292 (2023).
23. Y. Weng, Y. Zhang, W. Wang, *et al.*, "High-efficiency and compact two-dimensional exit pupil expansion design for diffractive waveguide based on polarization volume grating," *Opt. Express* **31**(4), 6601–6614 (2023).
24. Y. Weng, Y. Zhang, J. Cui, *et al.*, "Liquid-crystal-based polarization volume grating applied for full-color waveguide displays," *Opt. Lett.* **43**(23), 5773–5776 (2018).
25. Y. Ding, Y. Li, Q. Yang, *et al.*, "Design optimization of polarization volume gratings for full-color waveguide-based augmented reality displays," *J. Soc. Inf. Disp.* **31**(5), 380–386 (2023).
26. Y. Ding, Y. Gu, Q. Yang, *et al.*, "Breaking the in-coupling efficiency limit in waveguide-based AR displays with polarization volume gratings," *Light: Sci. Appl.* **13**(1), 185 (2024).
27. Y. Gu, Y. Weng, R. Wei, *et al.*, "Holographic Waveguide Display with Large Field of View and High Light Efficiency Based on Polarized Volume Holographic Grating," *IEEE Photonics J.* **14**(1), 7003707 (2022).
28. C. Yang, R. Wei, W. Yang, *et al.*, "Simulation of gradient period polarization volume gratings for augmented reality displays," *Opt. Express* **32**(12), 21243–21257 (2024).
29. R. Ozaki, K. Saiki, S. Hashimura, *et al.*, "Geometrical Optics Analysis of Diffraction in Patterned Cholesteric Liquid Crystals," *ACS Appl. Opt. Mater.* **2**(7), 1338–1346 (2024).

30. Y. Ding, Q. Yang, Y. Li, *et al.*, "Waveguide-based augmented reality displays: perspectives and challenges," *eLight* **3**(1), 24 (2023).
31. D. W. Berreman, "Optics in Stratified and Anisotropic Media: 4×4-Matrix Formulation," *J. Opt. Soc. Am.* **62**(4), 502–510 (1972).
32. S. Nishimura and H. Mazaki, "Viewing angle compensation of various LCD modes by using a liquid crystalline polymer film "Nisseki LC film"," *Liquid Crystals X, Proc. SPIE* **6332**, 633203 (2006).
33. M. Mitov, "Cholesteric Liquid Crystals with a Broad Light Reflection Band," *Adv. Mater.* **24**(47), 6260–6276 (2012).
34. M. Rafayelyan, G. Agez, and E. Brasselet, "Ultrabroadband gradient-pitch Bragg-Berry mirrors," *Phys. Rev. A* **96**(4), 043862 (2017).
35. Y. Huang, L. Lu, N. Diorio, *et al.*, "60-3: Invited Paper: Liquid Crystal Optics for AR/VR/MR Near Eye Displays," *Symp Digest of Tech Papers* **54**(1), 857–860 (2023).
36. J. Xiong and S. T. Wu, "Rigorous coupled-wave analysis of liquid crystal polarization gratings," *Opt. Express* **28**(24), 35960–35971 (2020).
37. Y. Li, T. Zhan, Z. Yang, *et al.*, "Broadband cholesteric liquid crystal lens for chromatic aberration correction in catadioptric virtual reality optics," *Opt. Express* **29**(4), 6011–6020 (2021).
38. K. Yin, H. Y. Lin, and S. T. Wu, "Chirped polarization volume grating with ultra-wide angular bandwidth and high efficiency for see-through near-eye displays," *Opt. Express* **27**(24), 35895–35902 (2019).